

Biocomputing based on particle disassembly

Maxim P. Nikitin^{1,2,3*}, Victoria O. Shipunova², Sergey M. Deyev^{2,4*} and Petr I. Nikitin¹

Nanoparticles with biocomputing capabilities could potentially be used to create sophisticated robotic devices with a variety of biomedical applications, including intelligent sensors and theranostic agents. DNA/RNA-based computing techniques have already been developed that can offer a complete set of Boolean logic functions and have been used, for example, to analyse cells and deliver molecular payloads. However, the computing potential of particle-based systems remains relatively unexplored. Here, we show that almost any type of nanoparticle or microparticle can be transformed into autonomous biocomputing structures that are capable of implementing a functionally complete set of Boolean logic gates (YES, NOT, AND and OR) and binding to a target as result of a computation. The logic-gating functionality is incorporated into self-assembled particle/biomolecule interfaces (demonstrated here with proteins) and the logic gating is achieved through input-induced disassembly of the structures. To illustrate the capabilities of the approach, we show that the structures can be used for logic-gated cell targeting and advanced immunoassays.

The processing of input information is key to the intelligence of any robot. For biomedical robots the inputs are biomolecules, and analysis of these biochemical data will be crucial to the successful use of such devices in the diagnosis of disease. Medical disorders can be characterized in the body by irregular levels of specific molecules, including soluble entities circulating in the blood (for example, high glucose/low insulin as an indication for diabetes), interstitial fluids (for example, chemokines for inflammation), receptors expressed on the cell surface (for example, HER2/neu for several cancers) and molecules inside cells (for example, foreign DNA for viral infections). However, a disorder can rarely be identified unambiguously by a single irregular factor, so an autonomous device requires biocomputing capabilities to analyse several biomolecular cues simultaneously in order to identify a particular disorder.

Computation inside cells^{1,2} is possible using complex cellular DNA/RNA-processing machinery, which can analyse the state of a cell and induce apoptosis³, for example. Outside cells, alternative biocomputing methods are required. Over the last two decades a number of approaches have been suggested^{1,2,4} that perform computation with molecules alone (DNA/RNA^{5–13}, proteins¹⁴, peptides¹⁵ or small molecules¹⁶) or also with involvement of nanoparticles or microparticles^{17–25}. Currently, DNA/RNA-based techniques are the only ones to offer a complete set of Boolean functions for the same two inputs. These DNA/RNA methods have been applied to various mathematical tasks, such as solving algebraic problems¹³ and playing the game ‘tic-tac-toe’⁷. They have also been used for biomedical purposes. In particular, molecular cascades of DNA strand displacement reactions have recently been used to evaluate cells through Boolean analysis of their surface markers^{26,27}.

Nanoparticles have a variety of intrinsic features²⁸ that are not available in molecules (for example, controllability by magnetic fields, size-tunable photoemission, and photoluminescence based on energy transfer upconversion) and have significant potential in biomedical applications. By adding biocomputing capabilities to such materials, their behaviour could be placed under logic control, and robotic devices could be created to take advantage of these attractive intrinsic features. To meet these ends, logic-gated

nanorobots have been developed that can carry small payloads and target cells²⁹. In this approach, an all-in-one DNA origami barrel design allows the payloads—several Fab antibody fragments or 5 nm gold nanoparticles—to be delivered to target cells upon AND-type activation by two inputs. Alternatively, nanoparticle-based systems have been reported that allow payload release from nanoparticle pores, for example, based on AND logic gating using light and pH as inputs²² and OR gating using K⁺ and heating as inputs²³. Nevertheless, the computing potential of all-in-one particle-based systems (and non-DNA approaches in general) remains to be addressed.

Design and operation of biocomputing structures

Figure 1 presents the design of our particle-based biocomputing structures. The logic gating functionality is built into specifically designed interfaces that can be self-assembled on virtually any nanoparticle/microparticle (referred to here as the ‘core’ particle) as a sensory, decision-making and targeting corona. This feature provides a generality to the platform in terms of the size, nature and number of particles that can be incorporated into the structures as payload. The output action to be performed by the core particle as a result of logic gating is produced by an output receptor that mediates its interaction with a certain target (output receptor’s ligand). The output receptor can be, for example, a targeting molecule for logic-gated delivery of the core particles to diseased cells, or a toxic enzyme for inducing cells’ death.

Basic single-input YES and NOT logic gates are defined by two essentially different designs of signal transduction between the input and output molecular systems. In the YES gate (Fig. 1a), the output and input receptors are co-localized on the surface of the core particle. During assembly of the biocomputing structure, the output receptor is sterically shielded^{18,30} from interaction with its ligand by ‘shielding’ particles, which are assembled on the core particle via an input receptor–ligand bond. Following an input action, which destroys this bond, the structure disassembles, making the output receptor accessible to the output receptor’s ligand and, hence, allowing the output action. We demonstrate in the following that even large 100 nm shielding particles can be used, providing sufficient flexibility in terms of the

¹Prokhorov General Physics Institute, Russian Academy of Sciences, Natural Science Centre, 38 Vavilov St, Moscow 119991, Russia, ²Shemyakin-Ovchinnikov Institute of Bioorganic Chemistry, Russian Academy of Sciences, 16/10 Miklukho-Maklaya St, Moscow 117997, Russia, ³Moscow Institute of Physics and Technology, 9 Institutskii per., Dolgoprudny, Moscow Region 141700, Russia, ⁴Lobachevsky State University of Nizhny Novgorod, 23 Gagarin Av., Nizhny Novgorod 603950, Russia. *e-mail: max.nikitin@phystech.edu; deyev@ibch.ru

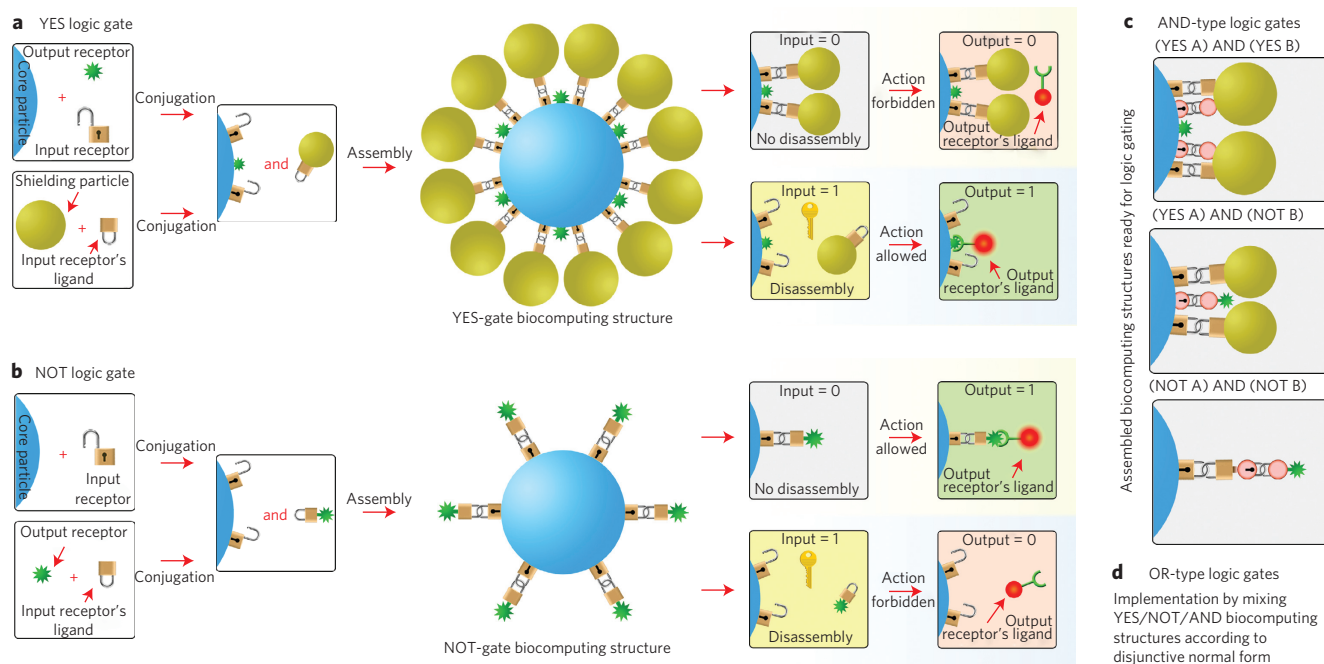


Figure 1 | Conceptual designs of biocomputing structures for YES/NOT/AND/OR logic basis. **a, b**, Assembly and performance of biocomputing structures for a YES gate (**a**) and a NOT gate (**b**). **c**, Design of three different AND-type logic gates based on YES/NOT. **d**, OR gates are realized by mixing of structures for YES/NOT/AND operands. Input-processing interfaces in **a–c** are denoted as locks to illustrate the indifference of the concept to the biochemical nature of interfaces and inputs. Rectangular and round locks represent interfaces that process different inputs.

size and localization of receptors that can be shielded. In the NOT gate (Fig. 1b), the core particle carries only an input receptor to allow assembly with the input receptor's ligand conjugated with the output receptor. On being subjected to an input, the output receptor disassembles from the core particle. Accordingly, the core particle can bind the output receptor's ligand only if no input is present.

Double-input logic gates are realized as follows. Three principally different AND functions can be constructed using YES/NOT gates: (YES A) AND (YES B) = AND gate, (YES A) AND (NOT B) = INHIBIT gate, (NOT A) AND (NOT B) = NOR gate. These are implemented by a combination of respective YES/NOT operands on the surface of a single core particle (Fig. 1c). Using the disjunctive normal form³¹, any arbitrary logic function can be presented as the OR gate with YES/NOT/AND operand gates; for example, [IF A THEN B] = [(NOT A) OR (YES B)], [A XOR B] = [(YES A) AND (NOT B)] OR [(NOT B) AND (YES B)] and so on. These functions are straightforwardly realized by mixing the respective YES/NOT/AND-type structures, each of which contribute to the net output action (Supplementary Note 1).

Importantly, all the proposed designs equip each structure with all means to perform the computation and implement the output action on its own without interaction with any entities except inputs and targets. As a result, the performance of the structures is independent of their concentration.

One of the notable advantages of the approach is the wide range of possible inputs and input-processing interfaces with which the system can be built. In contrast to many advanced biocomputing approaches anchored to DNA complementarity, the design of the biocomputing corona provides flexibility and independence from the biochemical nature of its constituents. To highlight this feature we demonstrate here a protein-based biocomputing system that allows completely DNA/RNA-free implementation of a full set of Boolean functions.

Logic gates in different experimental set-ups

The performance of YES gates based on diverse proteinaceous input-processing interfaces depending on the concentrations of

the respective inputs is shown in Fig. 2. For examples of NOT gates see Supplementary Fig. 1. To construct these structures we used 3 μm magnetic particles (Spherotech) as the core particles because they can be non-invasively observed by optical microscopy for unambiguous verification of the steric hindrance of every individual core particle by the corresponding shielding particles (rather than steric hindrance due to aggregation of core particles) (Fig. 3b, Supplementary Fig. 2). Several types of nanoparticle were tested as shielding particles. In spite of having quite similar behaviour during directed self-assembly onto the core particle³², the nanoparticles presented different disassembly performances. Polystyrene particles, for example, demonstrated highly specific assembly but only slight disassembly, even under harsh protein-denaturing conditions³³. Superparamagnetic iron-oxide carboxymethyl-dextran (CMD)-coated nanoparticles (SPIONs) synthesized using a standard co-precipitation route (see Supplementary Section 'Synthesis of SPIONs') exhibited the best disassembly. However, the magnetism of the SPIONs may affect assembly with the magnetic core particle. To avoid this, we synthesized paramagnetic iron oxyhydroxide (ferrihydrite³⁴) CMD-coated nanoparticles (FH-particles; see Supplementary Section 'FH-particle synthesis and characterization' and Supplementary Figs 3–11). Because they have the same coating, these particles demonstrated shielding behaviour similar to SPIONs, but were inert to magnetic field gradients.

The biocomputing structures were self-assembled by mixing core and shielding particles conjugated with the respective receptors (as the model output receptor we used biotin conjugated with carrier proteins in all cases except for streptavidin–iminobiotin structures, which utilized human IgG as the output receptor). The biocomputing performance of the assembled structures was assessed by 1 h incubation of the structures with the respective inputs (for gate kinetics see Supplementary Fig. 12), after which they were allowed to interact with the corresponding output receptor's ligand: streptavidin (STR) or protein A (PrA) immobilized simultaneously with horseradish peroxidase (HRP) on FH-particles (FH-STR:HRP or FH-PrA:HRP, respectively). Binding of the core particle with the output receptor's ligand was quantified by a chromogenic HRP assay.

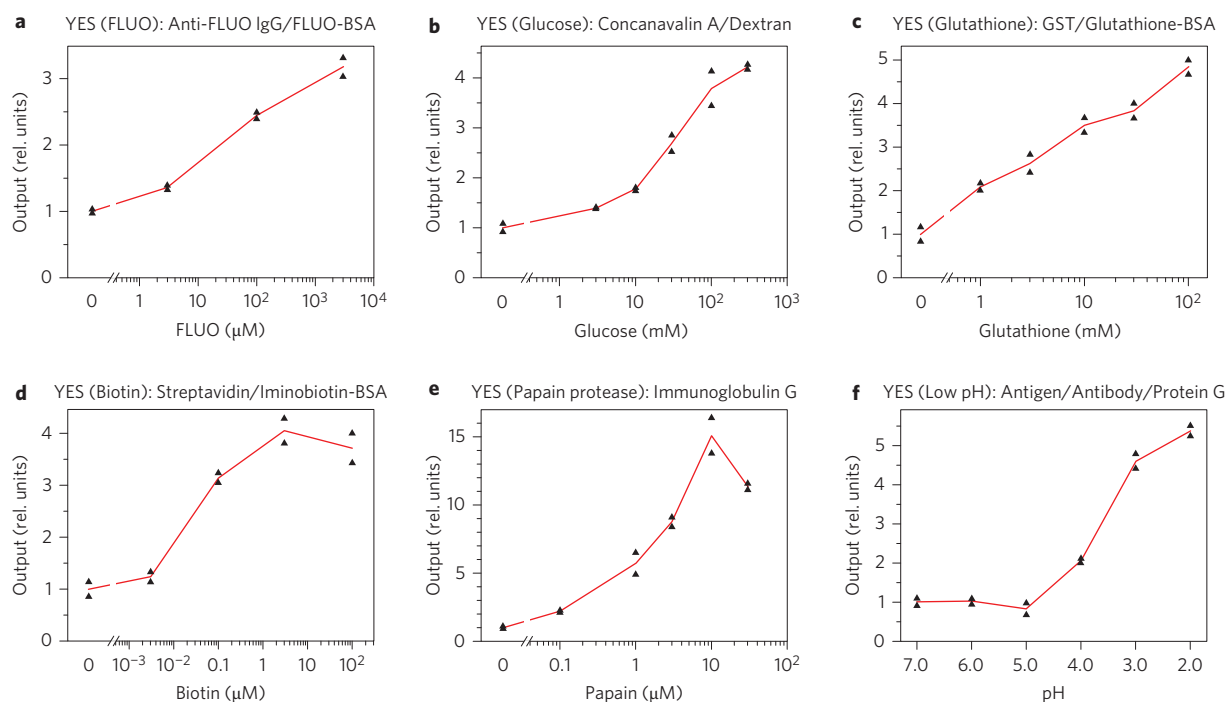


Figure 2 | Dependences of output on input concentration for YES gates implemented with different protein-based input-processing interfaces.

a–f. Gates sensitive to: **a**, fluorescein hapten (FLUO) using antibody/antigen interface (anti-FLUO antibody/FLUO conjugated with bovine serum albumin, BSA); **b**, glucose using lectin/carbohydrate interface (concanavalin A/dextran); **c**, glutathione using enzyme/substrate interface (glutathione S-transferase (GST)/glutathione conjugated with BSA); **d**, biotin using streptavidin/imminobiotinylated BSA interface; **e**, proteinase papain using proteolysis-susceptible bond (immunoglobulin G); **f**, low pH using non-covalent pH-susceptible protein bond (protein G/antibody/antigen). The output decrease for 30 μM papain (**e**) is possibly due to proteolysis of the output receptor (biotinylated Fab fragment of non-specific IgG). In **a–f**, pairs of triangles depict duplicate performance of the assembled biocomputing structures, and the red line connects the average values. Absorbance signals are normalized by average signals corresponding to the ‘No input’ condition: zero input concentration (**a–e**) or pH 7.0 (**f**). Results are representative of at least three independent experiments (each performed in duplicate) with independently assembled structures.

We focused here on protein-based input processing and did not test other non-protein interfaces such as those based on DNA, synthetic receptors or chemical bonds. However, we do not anticipate any conceptual obstacles to constructing the corona using any other interface provided that the corresponding inputs can break the relevant bonds and cause disassembly.

In the following experiments we used antibody-based interfaces that can be adapted easily to the processing of many biomedical markers. As model inputs we chose the antibiotic chloramphenicol (CAP), which is relevant for food safety diagnostics, and fluorescein (FLUO) label in the form of the fluorescein isothiocyanate–ethanolamine conjugate. Anti-CAP antibody with chloramphenicol–protein conjugates and anti-FLUO antibody with fluorescein isothiocyanate–protein conjugates served as the input-processing interfaces.

To demonstrate the versatility of the approach in terms of output actions, sizes and types of output receptors, core and shielding particles, we implemented the YES/NOT gates for CAP in several different set-ups (Fig. 3). Figure 3a shows both single-input gates for CAP in the set-up already described. Similar gate performances were achieved with the anti-CAP antibody immobilized on the core particle (direct format) or on the shielding particle (inverse format), although the former option required oriented antibody immobilization via protein G. The feasibility of the steric shielding of receptors as large as immunoglobulin G molecules, whose size spans the dimensions of most commonly used bioreceptors, was verified (Supplementary Note 2, Supplementary Fig. 13). A similar set-up with 3 μm core and FH shielding particles but with streptavidin-conjugated 200 nm fluorescent particles (Spherotech) as the output receptor’s ligand was used to prove the

individual steric hindrance and performance of each biocomputing structure (Fig. 3b).

To demonstrate the applicability of the approach for smaller core particles (100 nm hydrodynamic size) and illustrate the possibility of output action as an interaction with the solid phase, we chose two conventional immunoassay set-ups. A qualitative lateral flow assay that is used widely for the detection of drugs of abuse, antibiotics, pesticides, and so on was selected as the first option. Biocomputing structures were assembled using FH core particles, the binding of which with anti-antibiotin antibody on a test-line of test strips was considered as the output (Fig. 3c). Anti-CAP antibody was used for steric shielding of biotin conjugated with CAP–BSA. Remarkably, the YES gate embodies an immunoassay that exhibits higher particle binding on the test-line at higher input concentrations. Traditional particle-based lateral flow competitive immunoassays feature the opposite dose–response behaviour, and therefore more difficult measurement of small changes in high signal at low input concentrations near the detection limit. Therefore, the proposed YES gate is attractive as an alternative to the conventional lateral flow assay. In the second quantitative set-up we performed an immunoassay with three-dimensional fibre solid-phase and magnetic labels^{35–37}, which used SPIONs instead of FH-particles as the core particles. After exposure to inputs, the biocomputing structures were passed through the three-dimensional fibre filters with sorbed anti-antibiotin antibodies (Supplementary Fig. 14). The number of structures bound to the solid phase was measured by the method of magnetic particle quantification by their nonlinear magnetization (MPQ)^{35–39} (Fig. 3d). For a detailed description of the experimental set-ups and construction of the biocomputing structures see Supplementary Sections ‘Assembly of

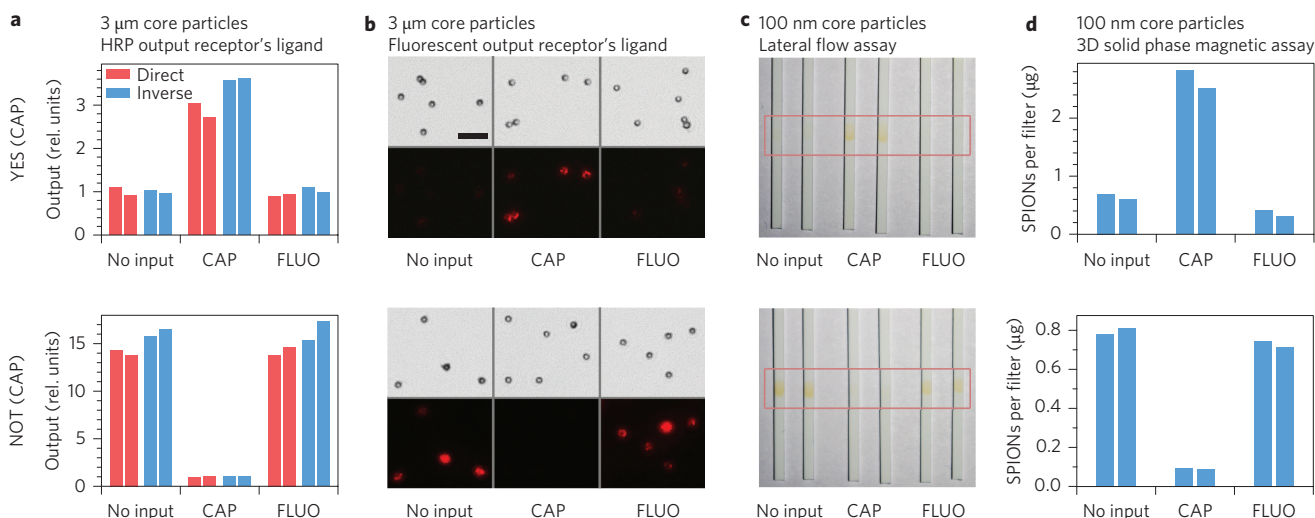
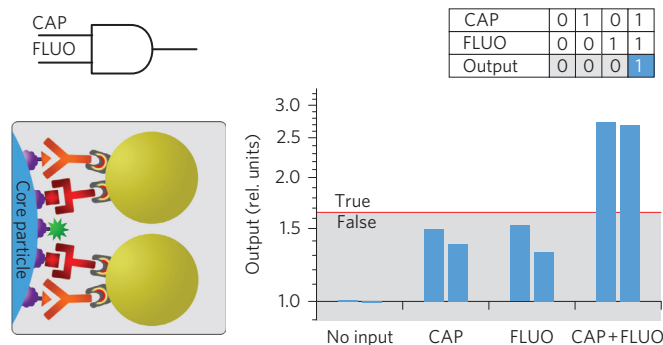
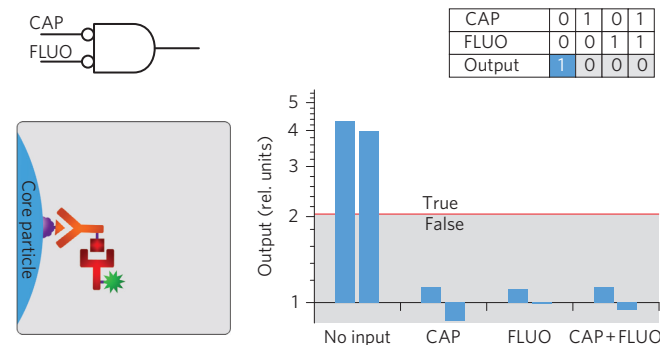


Figure 3 | YES/NOT gates for CAP in different experimental set-ups. **a**, Set-up with 3 μm core particles, FH-HRP:STR output receptor's ligand, and quantitative peroxidase assay for output signal readout. Performance of structures constructed in direct (red) and inverse (blue) formats. **b**, Set-up with 3 μm core particles and fluorescent particle conjugated with STR as the output receptor ligand. Individual operation of biocomputing structures demonstrated by bright-field and corresponding fluorescent images. Scale bar, 15 μm. **c**, Qualitative lateral flow set-up with 100 nm core FH-particles. Red rectangles show the region of the test strips with test-lines with sorbed antibody. **d**, Quantitative three-dimensional fibre solid-phase immunoassay set-up with 100 nm SPION core particles. Duplicate performance of the assembled biocomputing structures is represented as pairs of bars (**a,d**) and lateral flow test strips (**c**). In **a**, absorbance signals are normalized by the corresponding 'No input' signal (YES gate) and 'CAP' signal (NOT gate) averaged for the duplicate values. Results are representative of at least two independent experiments (each performed in duplicate) with independently assembled structures.

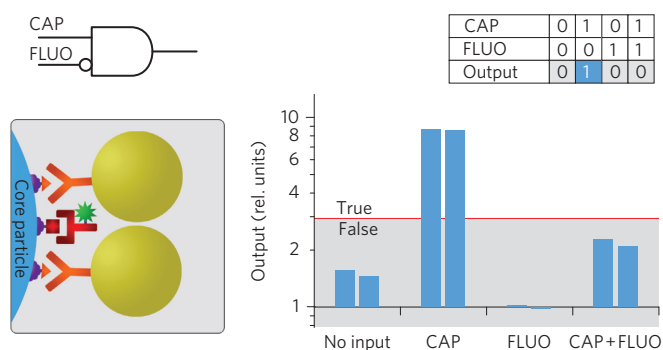
a (YES CAP) AND (YES FLUO) ≡ AND gate



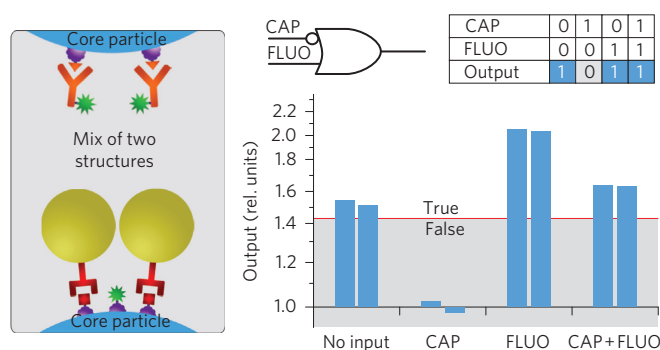
c (NOT CAP) AND (NOT FLUO) ≡ NOR gate



b (YES CAP) AND (NOT FLUO) ≡ INHIBIT gate



d (NOT CAP) OR (YES FLUO) ≡ IF-THEN gate



● Shielding particle ◐ Protein A/G/L ● BSA ★ Biotin label ◐ Interfaces: ◐ Anti-CAP IgG / ◐ CAP label ◐ Anti-FLUO IgG / ◐ FLUO label ◐ Inputs: ◐ Free CAP ◐ Free FLUO

Figure 4 | Double-input gates in the set-up with 3 μm core particles, FH-HRP:STR output receptor's ligand, and quantitative peroxidase assay for output signal readout. **a-d**, Scheme of the assembled structures ready for logic gating (left) and results in a log scale (right). Duplicate performance of the assembled biocomputing structures is represented by pairs of bars. Signals are normalized by each gate's minimum output (average of the duplicate values). Results are representative of at least two independent experiments (each performed in duplicate) with independently assembled structures.

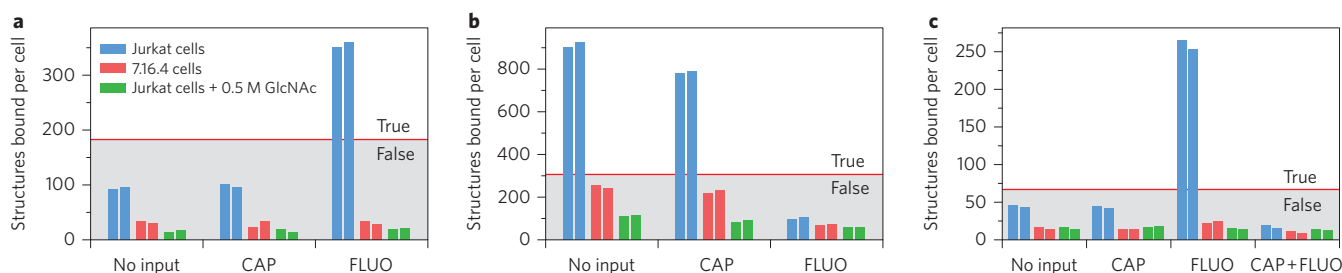


Figure 5 | Cell targeting as the output action of logic gating. a–c. Cell-bound structures were quantified by the method of magnetic particle quantification by their nonlinear magnetization (MPQ). The number of structures bound per cell depending on the input is shown for single-input gates, YES(FLUO) (a) and NOT(FLUO) (b), and for an example of double-input gate (YES FLUO) AND (NOT CAP) (c). Jurkat cells, 7.16.4 cells and Jurkat cells in the presence of 0.5 M GlcNAc were targeted. Duplicate performance of the assembled biocomputing structures is represented by pairs of bars. For each gate, the true/false threshold is the geometric mean of the maximum and minimum outputs (averages of the corresponding duplicate values) for labelling target Jurkat cells. Results are representative of at least two independent experiments (each performed in duplicate) with independently assembled structures.

CAP&FLUO biocomputing structures’, ‘Performance of CAP&FLUO biocomputing structures as logic gates’ and ‘Assembly and performance of biocomputing structures for other inputs’.

Double-input logic gates were implemented using 3 μm core particles and FH-STR:HRP output receptor’s ligand in the set-up used for the experiments shown in Figs 2 and 3a. Realizations of all the above-mentioned AND-type gates (AND, INHIBIT, NOR) are presented in Fig. 4. In contrast to the YES/NOT gates, double-input gates have several possible disassembly routes, which depend on four input combinations and yield different outputs. It is common sense to regard the maximum and minimum outputs as ‘true’ and ‘false’, respectively. However, for classification of the intermediate outputs in terms of Boolean logic, a true/false threshold should be defined. Considering the standard semi-logarithmic dose–response behaviour of many drugs (response proportional to logarithm of dose) and taking into account that the output of our system is proportional to the number of ‘activated’ core particles, we define the threshold as the geometric mean of the gate’s maximum and minimum outputs. This threshold corresponds to the dose of the ‘activated’ core particles that would cause the average response (Supplementary Note 3). For the implementation of OR-type gates it is essential to equalize the contribution to the output of each type of participating biocomputing structure either by mixing them in the amounts inversely proportional to their maximum outputs or by adjusting the density of the output receptors on the surface of the core particles. An example of OR-type gate is shown in Fig. 4d for (NOT CAP) OR (YES FLUO) gate implemented by mixing YES(FLUO) and NOT(CAP) biocomputing structures in a 1:4.6 ratio to equalize their contribution to the output.

Reproducibility of the gates was verified by independent experiments with biocomputing structures assembled using independently conjugated particles. Due to the differences in particle conjugation and structure assembly, the inter-assay variations were significantly larger than the intra-assay ones. Despite variations in the absolute values, the inter-assay performance of the gates proved to be reliable in terms of Boolean logic classification (Supplementary Note 4, Supplementary Figs 15 and 16).

Logic-gated cell targeting

Now let us consider ‘programming’ the structures for a more complex biorobotic task, namely, targeting specific cells based on logic-gated analysis of soluble biomolecular inputs. As we have noted already, soluble inputs can provide valuable information for autonomous agents because organisms use blood and other body fluids to transmit a vast amount of biochemical information between cells. Tapping these data streams may permit the agents to recognize certain diseases (for example, diabetes) and processes

(such as inflammation and angiogenesis), while the ability to use the output receptor to target cells specifically (or non-specifically) as the output action provides secondary treatment control, for example, to neutralize the pathogenic cells responsible for inflammation.

Magnetic nanoparticles (100 nm, Chemicell) coated with glucuronic acid (ARA-particles) were used as the core particles. As the model targeting output receptor we used wheat germ agglutinin (WGA), one of the widely used lectins for targeting cells with a specific glycosylation profile⁴⁰. WGA specifically binds *N*-acetyl-D-glucosamine (GlcNAc) and sialic acid carbohydrate residues. Human leukemic Jurkat T-cells that express WGA-specific carbohydrates were selected as the target cells. As the proof-of-concept, both basic single-input YES(FLUO) and NOT(FLUO) gates were demonstrated, as well as an example of a double-input gate, (YES FLUO) AND (NOT CAP) (Fig. 5). The biocomputing structures were incubated with input solutions and mixed with cell suspensions, then the cell-bound structures were quantified by the MPQ method. The drastic change in the outer surfaces of the structures as a result of input-induced disassembly did not practically affect the non-specific interactions of the structures with cells. The specificity of cell targeting was verified by testing the interaction of the same structures with Jurkat cells in the presence of WGA-inhibiting monosaccharide (GlcNAc), as well as with ‘non-specific’ hybridoma 7.16.4 cells, whose interaction with WGA was very weak due to the different glycosylation profile (Supplementary Fig. 17). In these control experiments, the biocomputing structures showed much lower binding with cells, exhibiting a false output in all mentioned cases, as well as no or little input-induced variation in binding (Fig. 5).

Conclusions

Upon computation, the proposed biocomputing structures can target a wide range of entities, from molecules bound with the solid phase to nanoparticles and living cells, suggesting the great potential of the platform for diverse operational modes. The approach is mainly oriented to the processing of soluble inputs and, in principle, inputs of a physical nature, such as light and temperature. Being mainly suitable for computation outside cells, the approach efficiently supplements two other types of biocomputing method that operate at the cell surface and inside cells. In fact, with a combination of these methods one can imagine a biocomputing structure that, with a logical analysis of blood markers, targets cells with a particular surface profile pre-labelled by molecular DNA strand displacement cascades^{26,27} and delivers genes that logically evaluate the cell’s state through in-cell biocomputing^{1–3}.

The multiparametric nature of the presented platform offers ample opportunities for further development: from optimizing the

biochemical and physical properties of nanoparticles to choosing the best receptors. For example, because biocomputing depends on dissociation of the participating bonds (in the case of non-covalent bonds), balancing the affinity of the involved receptors is important. The bond should be tight enough to be preserved in the absence of input but not too tight to forbid input interference. Receptors with relatively low affinity and high avidity may be the most attractive option. Fan-out can be increased easily by simultaneous conjugation of several output receptors with the core particle. Gate construction with higher fan-in as well as more complex OR gating may be more challenging. Specifically, although the NOT-type gating should not cause substantial problems (see, for example, the virtually perfect multi-input gating in Fig. 4c), the YES-type gating may require enhancement of the steric shielding efficiency (note, for example, the significant variations in the false values in Fig. 4a,b). To increase the true/false output ratio for YES-type gating and equalize false values in YES-AND-NOT gating, it is important to shield every single output receptor. This can be realized by the high-density immobilization of input receptors on core particles with a developed surface and by using input receptors that do not allow disassembly in the absence of inputs. YES-AND-YES gating may be substantially enhanced by state-of-the-art multivalent genetically engineered fused receptors or aptamers to guarantee that each shielding particle is bound to the core particle by all participating input-processing interfaces simultaneously (Supplementary Note 5, Supplementary Fig. 18). Cascading of the logic gates may be plausible with employment of hydrolase enzymes as the output receptors. For example, shielding of glucosidase from a macromolecular carbohydrate substrate (such as dextran-based coating of FH-particles) would inhibit cleavage of glucose, which can be an input for the following logic gate.

Our biocomputing structures, which are based on stimuli-responsive composite nanoparticle/biomolecule interfaces, allow remarkably complex information processing. Signal transduction between several orthogonal receptors that do not share any specific biochemistry is achieved, among other means, by spatial entanglement of the receptors. The proposed platform can be applied to the development of autonomous nanodevices as intelligent biosensors with built-in biochemical data analysis for multiplex point-of-care diagnostics, field testing and so on. Furthermore, with the progress in metabolomics for the identification of new small-molecule biomarkers, the platform could be used to construct bionanorobotic agents for complex stimuli-controlled targeted drug delivery, early diagnostics and health monitoring as a part of preventive medicine solutions.

Methods

Synthesis and characterization of FH-particles and SPIONs. FH-particles were synthesized by the precipitation of iron(III) chloride in alkali conditions, and SPIONs by co-precipitation of iron(II) and (III) chloride salts. Nanoparticles peptized by HNO₃ and washed with water were coated with CMD (for detailed protocols see Supplementary Sections 'FH-particle synthesis and characterization' and 'Synthesis of SPIONs'). Dynamic light scattering showed the hydrodynamic sizes of CMD-coated FH-particles and SPIONs to be 104 ± 36 nm and 109 ± 32 nm, respectively. The FH-particles were characterized in detail by X-ray diffraction, transmission electron microscopy, Fourier transform infrared spectroscopy and Mössbauer spectroscopy (see Supplementary Section 'FH-particle synthesis and characterization' and Supplementary Figs 3–9).

FLUO, biotin, iminobiotin, CAP and glutathione (GSH) labelling. Labelling by fluorescein isothiocyanate, NHS-biotin, NHS-iminobiotin was performed according to manufacturers' recommendations with variations; CAP labelling was carried out by carbodiimide conjugation of succinylated CAP, and GSH was conjugated via its thiol group to the amino group of BSA (see Supplementary Sections 'FLUO, biotin and iminobiotin labelling', 'CAP labelling', 'Conjugation with GSH').

Protein conjugation with particles. Protein conjugation was performed via carbodiimide activation of the carboxy groups of the particles. For detailed protocols and testing of conjugates specificity, see Supplementary Section 'Protein conjugation with nanoparticles', Supplementary Table 1 and Supplementary Figs 10 and 11.

Epifluorescent/optical microscopy. Samples of biocomputing structures based on 3 μm core particles were studied with an inverted epifluorescent microscope (Carl Zeiss Axiovert 200). A 3–5 μl sample was dropped onto a microscope slide, and the structures were settled using a magnet and visualized in bright field and, when applicable, upon excitation of the fluorophore of fluorescent particles (at 565/630 nm).

Detection of magnetic particles. Detection was performed by the MPQ method, as reported previously^{35–39}. Briefly, magnetic particles are subjected to a magnetic field generated at one or two frequencies f_1 , f_2 and the particle response measured on a combinatorial frequency $f = n \cdot f_1 + m \cdot f_2$, where n and m are integers (one of them can be zero). The MPQ method is insensitive to linear dia- and paramagnetic materials.

Assembly and performance of biocomputing structures. Briefly, the structures were constructed as follows. YES(Glucose) and YES(Biotin) gates: core particles were conjugated with concanavalin A & biotinylated BSA or iminobiotinylated BSA & human IgG, respectively and shielded by raw FH-particles (glucose-gate) or streptavidin-conjugated FH-particles (biotin-gate). YES(Glutathione): core particles conjugated with BSA labelled with biotin & GSH were shielded by FH-particles with GST. YES(Low pH): core particles with FLUO-BSA & biotinylated BSA were first assembled with anti-FLUO antibody and shielded by protein-G-functionalized FH-particles. YES(Papain) structures were constructed similarly but used FLUO and biotin labelled Fab antibody fragments on the core particle to minimize detachment of biotin due to proteolysis of the carrier protein. The structures for CAP & FLUO gates based on 3 μm core particles were assembled in the following way. In the direct YES(CAP), anti-CAP antibody and biotinylated non-specific IgG were immobilized on the core particles via protein G. The shielding FH-particle was conjugated with CAP-BSA. The direct NOT gate used the core particles with anti-CAP antibody bound via protein G, while biotinylated CAP-BSA was used as the 'output receptor-input receptor ligand' conjugate. For the inverse format, the core particle was conjugated either simultaneously with CAP-BSA and biotinylated BSA for the YES gate or only with CAP-BSA for the NOT gate. Anti-CAP antibody was directly immobilized on the FH shielding particle. In the NOT gate, the 'output receptor-input receptor ligand' conjugate represented biotinylated anti-CAP antibody. FLUO gates were constructed similarly (Fig. 2 shows the inverse YES(FLUO) gate). The NOT gate with FH and SPION core particles was constructed as with 3 μm core particles, but for the YES gate, anti-CAP antibody was used as the shielding particle, while CAP & biotin were simultaneously conjugated with BSA before its immobilization on the core particle. Double-input gates for the FH-STR:HRP output receptor's ligand set-up were constructed in the following way. (YES CAP) AND (YES FLUO): core particle conjugated with both input receptors (CAP-BSA, FLUO-BSA) and output receptor (biotinylated BSA) was first assembled with anti-CAP and anti-FLUO antibody mixture and then with shielding FH-particles conjugated with protein A/G/L. (YES CAP) AND (NOT FLUO): core particle conjugated with both input receptors (CAP-BSA, FLUO-BSA) was first assembled with biotinylated anti-FLUO antibody and then with shielding FH-particles conjugated with anti-CAP antibody. (NOT CAP) AND (NOT FLUO): core particle conjugated with CAP input receptor (CAP-BSA) was first assembled with anti-CAP antibody labelled with FLUO and then with biotinylated anti-FLUO antibody. (NOT CAP) OR (YES FLUO) logic gate was implemented by a mixture of YES(FLUO) and NOT(CAP) structures at a 1:4.6 ratio. Biocomputing structures for cell targeting were designed as follows. YES(FLUO) gate: ARA-particles conjugated with FLUO-WGA and shielded by anti-FLUO antibody. NOT(FLUO) gate: ARA-particles conjugated with anti-FLUO antibody and assembled with FLUO-WGA. (YES FLUO) AND (NOT CAP) gate: ARA-particle conjugated with anti-CAP antibody, then assembled with WGA labelled with CAP and FLUO and, finally, shielded with anti-FLUO antibody. Detailed protocols for the assembly of the biocomputing structures as well as for the evaluation of their logic-gating performance are provided in the Supplementary Information.

Received 27 August 2013; accepted 2 July 2014;
published online 17 August 2014

References

- Benenson, Y. Biomolecular computing systems: principles, progress and potential. *Nature Rev. Genet.* **13**, 455–468 (2012).
- Miyamoto, T., Razavi, S., DeRose, R. & Inoue, T. Synthesizing biomolecule-based Boolean logic gates. *ACS Synth. Biol.* **2**, 72–82 (2013).
- Xie, Z., Wroblewska, L., Prochazka, L., Weiss, R. & Benenson, Y. Multi-input RNAi-based logic circuit for identification of specific cancer cells. *Science* **333**, 307–311 (2011).
- Katz, E. *Biomolecular Information Processing: From Logic Systems to Smart Sensors and Actuators* (Wiley, 2012).
- Adleman, L. M. Molecular computation of solutions to combinatorial problems. *Science* **266**, 1021–1024 (1994).
- Mao, C., LaBean, T. H., Relf, J. H. & Seeman, N. C. Logical computation using algorithmic self-assembly of DNA triple-crossover molecules. *Nature* **407**, 493–496 (2000).

7. Stojanovic, M. N. & Stefanovic, D. A deoxyribozyme-based molecular automaton. *Nature Biotechnol.* **21**, 1069–1074 (2003).
8. Benenson, Y., Gil, B., Ben-Dor, U., Adar, R. & Shapiro, E. An autonomous molecular computer for logical control of gene expression. *Nature* **429**, 423–429 (2004).
9. Rothmund, P. W., Papadakis, N. & Winfree, E. Algorithmic self-assembly of DNA Sierpinski triangles. *PLoS Biol.* **2**, e424 (2004).
10. Seelig, G., Soloveichik, D., Zhang, D. Y. & Winfree, E. Enzyme-free nucleic acid logic circuits. *Science* **314**, 1585–1588 (2006).
11. Elbaz, J. *et al.* DNA computing circuits using libraries of DNAAzyme subunits. *Nature Nanotech.* **5**, 417–422 (2010).
12. Pei, R., Matamoros, E., Liu, M., Stefanovic, D. & Stojanovic, M. N. Training a molecular automaton to play a game. *Nature Nanotech.* **5**, 773–777 (2010).
13. Qian, L. & Winfree, E. Scaling up digital circuit computation with DNA strand displacement cascades. *Science* **332**, 1196–1201 (2011).
14. Katz, E. & Privman, V. Enzyme-based logic systems for information processing. *Chem. Soc. Rev.* **39**, 1835–1857 (2010).
15. Ashkenasy, G. & Ghadiri, M. R. Boolean logic functions of a synthetic peptide network. *J. Am. Chem. Soc.* **126**, 11140–11141 (2004).
16. De Silva, A. P. & Uchiyama, S. Molecular logic and computing. *Nature Nanotech.* **2**, 399–410 (2007).
17. Liu, J. & Lu, Y. Smart nanomaterials responsive to multiple chemical stimuli with controllable cooperativity. *Adv. Mater.* **18**, 1667–1671 (2006).
18. Von Maltzahn, G. *et al.* Nanoparticle self-assembly gated by logical proteolytic triggers. *J. Am. Chem. Soc.* **129**, 6064–6065 (2007).
19. Frezza, B. M., Cockroft, S. L. & Ghadiri, M. R. Modular multi-level circuits from immobilized DNA-based logic gates. *J. Am. Chem. Soc.* **129**, 14875–14879 (2007).
20. Motornov, M. *et al.* 'Chemical transformers' from nanoparticle ensembles operated with logic. *Nano Lett.* **8**, 2993–2997 (2008).
21. Freeman, R., Finder, T. & Willner, I. Multiplexed analysis of Hg²⁺ and Ag⁺ ions by nucleic acid functionalized CdSe/ZnS quantum dots and their use for logic gate operations. *Angew. Chem. Int. Ed.* **48**, 7818–7821 (2009).
22. Angelos, S., Yang, Y. W., Khashab, N. M., Stoddart, J. F. & Zink, J. I. Dual-controlled nanoparticles exhibiting AND logic. *J. Am. Chem. Soc.* **131**, 11344–11346 (2009).
23. Wen, Y. *et al.* DNA-based intelligent logic controlled release systems. *Chem. Commun.* **48**, 8410–8412 (2012).
24. Huang, Z., Tao, Y., Pu, F., Ren, J. & Qu, X. Versatile logic devices based on programmable DNA-regulated silver-nanocluster signal transducers. *Chemistry* **18**, 6663–6669 (2012).
25. Chen, J., Fang, Z., Lie, P. & Zeng, L. Computational lateral flow biosensor for proteins and small molecules: a new class of strip logic gates. *Anal. Chem.* **84**, 6321–6325 (2012).
26. Rudchenko, M. *et al.* Autonomous molecular cascades for evaluation of cell surfaces. *Nature Nanotech.* **8**, 580–586 (2013).
27. You, M. *et al.* DNA 'Nano-claw': logic-based autonomous cancer targeting and therapy. *J. Am. Chem. Soc.* **136**, 1256–1259 (2014).
28. Xie, J., Lee, S. & Chen, X. Nanoparticle-based theranostic agents. *Adv. Drug Deliv. Rev.* **62**, 1064–1079 (2010).
29. Douglas, S. M., Bachelet, I. & Church, G. M. A logic-gated nanorobot for targeted transport of molecular payloads. *Science* **17**, 831–834 (2012).
30. Rubenstein, K. E., Schneider, R. S. & Ullman, E. F. 'Homogeneous' enzyme immunoassay. A new immunochemical technique. *Biochem. Biophys. Res. Commun.* **47**, 846–851 (1972).
31. Reeves, C. M. *An Introduction to Logical Designs of Digital Circuits* (Cambridge Univ. Press, 1972).
32. Nikitin, M. P., Zdobnova, T. A., Lukash, S. V., Stremovskiy, O. A. & Deyev, S. M. Protein-assisted self-assembly of multifunctional nanoparticles. *Proc. Natl Acad. Sci. USA* **107**, 5827–5832 (2010).
33. Aghayeva, U. F., Nikitin, M. P., Lukash, S. V. & Deyev, S. M. Denaturation-resistant bifunctional colloidal superstructures assembled via the proteinaceous barnase–barstar interface. *ACS Nano* **7**, 950–961 (2013).
34. Schwertmann, U. & Cornell, R. M. in *Iron Oxides in the Laboratory: Preparation and Characterization* 2nd edn, 103–112 (Wiley, 2000).
35. Nikitin, P. I. & Vetoshko, P. M. *Meter of magnetic susceptibility*. Russian patent no. RU2177611 (2000).
36. Nikitin, P. I. & Vetoshko, P. M. Analysis of biological and/or chemical mixtures using magnetic particles. Russian patent no. RU2166751 (2000), European patent no. EP1262766 (2001) and European patent no. EP2120041 (2001).
37. Orlov, A. V. *et al.* Magnetic immunoassay for detection of staphylococcal toxins in complex media. *Anal. Chem.* **85**, 1154–1163 (2013).
38. Nikitin, P. I., Vetoshko, P. M. & Ksenevich, T. I. New type of biosensors based on magnetic nanoparticle detection. *J. Magn. Magn. Mater.* **311**, 445–449 (2007).
39. Nikitin, M. P., Torno, M., Chen, H., Rosengart, A. & Nikitin, P. I. Quantitative real-time *in vivo* detection of magnetic nanoparticles by their non-linear magnetization. *J. Appl. Phys.* **103**, 07A304 (2008).
40. Gabor, F., Bogner, E., Weissenboeck, A. & Wirth, M. The lectin–cell interaction and its implications to intestinal lectin-mediated drug delivery. *Adv. Drug Deliv. Rev.* **56**, 459–480 (2004).

Acknowledgements

The authors thank A.V. Orlov (General Physics Institute, RAS) and P.M. Vetoshko (Institute of Radio Engineering and Electronics, RAS) for assistance with magnetic measurements, A.V. Zherdev and B.B. Dzantiev (Institute of Biochemistry, RAS) for providing the CAP antibody, and I.E. Deyev (Institute of Bioorganic Chemistry, RAS) for supplying GST.

Author contributions

M.P.N. conceived the idea, designed the study and performed the experiments. V.O.S. assisted with cell targeting experiments. M.P.N., S.M.D. and P.I.N. analysed data and wrote the manuscript.

Additional information

Supplementary information is available in the [online version](#) of the paper. Reprints and permissions information is available online at www.nature.com/reprints. Correspondence and requests for materials should be addressed to M.P.N. and S.M.D.

Competing financial interests

Two patent applications have been filed by M.P.N. (1) Nikitin, M.P. Logic element complex based on biomolecules (variants). Russian patent no. RU2491631, PCT application WO2013151465 (2012). (2) Nikitin, M.P. Method for determining the content of a ligand in a sample (alternatives). Russian patent no. RU2517161, PCT application WO2013151464 (2012).